Research Article

Shear Strength and Microstructure of Intact Loess Subjected to Freeze-Thaw Cycling

Kuan Liu [iD], Wanjun Ye, and Hongjun Jing [iD]

School of Architecture and Civil Engineering, Xi'an University of Science and Technology, Xi'an 710054, Shaanxi, China

Correspondence should be addressed to Kuan Liu; 19104053006@stu.xust.edu.cn

In the Loess Plateau, seasonal freeze and thaw cause great damage to the mechanical behavior and microstructure of soil, which leads to frequent geological disasters during winter and spring. To investigate the influence of freeze-thaw (FT) cycling (FTC) on the shear strength and microstructure of intact loess, triaxial shear, nuclear magnetic resonance, and scanning electron microscope tests were carried out on soil samples after target FT cycles. The results indicate that the FTC has limited changes to the soil stress-strain curve, but has a significant attenuation effect on the peak deviatoric stress. The peak deviatoric stress was attenuated by FTC but changed insignificantly after ten cycles. The cohesive force decays exponentially with the number of FT cycles, while the internal friction angle increases slightly. Moreover, under FTC, the T_2 hydrogen spectra of soil samples showed a multimodal distribution, with the main peak appearing to have two obvious upward shifts that occurred at 6 and 10 FT cycles. Indeed, a depolarization phenomenon related to the directional frequency of soil particles was observed, and the mass fractal dimension of the pore network increased slightly. In an FT environment, the shear strength declines due to accumulated internal microstructural damage. These findings contribute to a better understanding of the response of loess to FTC and provide novel ideas for the prevention of frost damage in loess areas.

1. Introduction

Loess is a type of Aeolian Quaternary sediment with loose structural features found between Western Europe and East Asia and from North America to South America [1, 2]. It covers 10% of the Earth's continental surface [1, 3]. In China, most of the loess is in seasonally frozen land areas. Seasonal changes in temperature cause changes in the physical and mechanical properties of soil, which is one of the crucial causes of geology-related engineering disasters [4–7]. To ensure the safety of construction and engineering operations, it is essential to understand the effects of freeze-thaw (FT) cycling (FTC) on the physical and mechanical properties of loess.

A literature review shows that research on the influence of FTC on soil physical properties has mainly focused on parameters such as density, particle size distribution, and permeability [8]. Under repeated FTC, different changes occur to the pore characteristics of soils with different initial densities. Loose soil becomes denser, and its porosity ratio decreases, whereas dense soil becomes looser and its porosity ratio increases [9, 10]. In terms of particle size, for both fine-grained soils (e.g., clay) and coarse-grained soils (e.g., sand), the FT effect decreases as the soil particle size increases [11]. Indeed, numerous studies have found increases in soil permeability following FTC in different regions, including Quebec, the Loess Plateau, and Hokkaido [12–14]. Nonetheless, there remain some important physical properties of natural loess in FT environments that have not been specifically studied, such as apparent integrity, dimension changes, and water migration in conventional samples. Research on the influence of FTC on the mechanical properties of soil has mainly focused on stress-strain performance, constitutive relationships, triaxial strength, and compression modulus [15]. Most studies report that the cohesion, compressive strength, and stiffness of soil attenuate to varying values as the number of FT cycles increases [16, 17]. Due to differences in test materials and conditions,

the mechanisms of change in soil shear strength properties due to FTC have not been completely unified [8]. Understanding these properties is important to engineering in seasonally frozen areas. In terms of shear strength parameters, several studies have reported that soil cohesion is reduced after FTC, while the friction angle increases slightly or does not change much [16, 18, 19].

In cold regions, geological disasters caused by FTC occur frequently and their mechanical mechanisms have received extensive attention [20, 21]. Practically, in freezing and thawing environments, the fundamental causes of change in the macroscopic mechanical properties of soil are changes to its microstructure [7, 8, 17]. These include deterioration in particle gradation, increases in porosity, and diminutions in cementation strength [22, 23]. Many widely accepted mechanisms have been proposed, such as the ice lens theory and the capillary stress concept [24, 25]. At present, numerous studies report that, under FTC, changes in the physical and mechanical parameters of soils are inseparable from their micro- and meso-scopic structure changes [26, 27]. Therefore, the multiscale structural features of soils subjected to FTC have also received attention. Computed tomography (CT), scanning electron microscopy (SEM), mercury intrusion porosimetry (MIP), and other technologies have been widely applied to the microscopic characterization of soil and rock [17, 20, 21]. This has led to several scholars adopting a range of image processing methods to quantitatively study the microstructures of various soils [26, 28–30]. However, the influences of the number of FT cycles and associated variations in soil water content on the soil microstructure (e.g., particles, pores, arrangement, and cements) remain unclear.

The abovementioned studies provide guidance for further understanding the physical-mechanical behavior and mechanisms of microstructural damage evolution in loess in seasonal FT regions. In general, however, there are very few studies focusing on soil water content and numbers of FT cycles that consider the complex nature of the climate and topography of the Loess Plateau. There has been little exploration of the macromechanical response mechanism related to the evolutionary characteristics of the microstructure of loess, which is urgently needed. Furthermore, studies of soil microstructure have mostly been conducted by methods that disturb the soil samples, making their results inconsistent. Recently, a nuclear magnetic resonance (NMR) method with low disturbance and sensitive response has been applied to the study of the pore characteristics of rock and soil masses, which has produced better results than previous methods (SEM and MIP) [29, 31, 32]. The NMR relaxation characteristics can provide valuable information on the natural loess structure in seasonal FT areas and are expected to supplement existing knowledge of the performance characteristics of soil structures during continuous FTC in the Loess Plateau.

Against this background, this study conducted FT tests on intact loess samples obtained from the Yan'an seasonal FT region of China. Triaxial tests, NMR tests, and SEM were used to determine the evolution in the macroscopic shear strength and microstructure of intact loess samples with different water contents under the action of FTC. The potential relationships and mechanisms related to the macrostrength and microstructure of soil subjected to FTC are then discussed.

2. Materials and Methods

2.1. Loess Sampling and Sample Preparation. The tested soil studied is a loess obtained from a foundation pit (36° 38′ 19″ N, 109° 29′ 33″ E) near Yan'an, Shaanxi province, China (Figure 1). This collection point was chosen because FTC is very common in this location during winter and spring, and the soil type is the most common one involved in earthwork in the Loess Plateau. Based on surface temperature information of Yan'an area collected by previous scholars [33], a sampling depth of 1.5–1.8 m was established as appropriate. The tested soil was classified as Late Pleistocene (Q_3) loess. They were cut into cylinders of roughly 20 mm height and 10 mm diameter, then stored in a sample bucket and sealed with cling-film and wax, placed in a wooden box with a sponge, and transported to the laboratory. Following geotechnical test standard [34], the basic physical characteristics of the soil samples were tested (Table 1). According to the Unified Soil Classification System (USCS), the loess was classified as clay of low plasticity (CL). Before preparing the intact loess samples, the spatial structure and mineral composition of the soil were examined by SEM (JSM-6390A, JEOL, Japan). It was found that the various group samples had extremely uniform structures (Figure 2). This ensured that the initial damage to the samples was homogeneous.

Investigations of the studied area showed that, during the period of winter freezing and spring thawing, the change range of water content of the soil was relatively large. This research focuses on two common water contents (18% and 22%) of the soil of this region. First, the collected intact soil blocks were precut into dimensions of 5 cm × 5 cm × 10 cm (length × width × height). Next, the precut soil blocks were weighed to estimate its initial water content, and then, they were moistened until they reached the target water content and finally placed into a humidor for 96 h to ensure the moisture was evenly distributed. They were then cut into cylindrical samples (76 mm in height and 38 mm in diameter) and sealed with the plastic film to prevent water loss. Note that, during cutting, the remaining residual soil was used to recheck the water content, and the error was controlled within ±0.1%. As per retests done on the samples, the average dry density and water content were 1.30 g/cm³ and 14.80%, respectively.

2.2. Experimental Design

2.2.1. Freeze/Thaw Tests. A high/low-temperature test device (RTP-175BU, Ruier test, China; Figure 3(a)) was used to simulate the closed (no water supplement) FT environment. The benefits of this FT scheme for clay have been widely explained [16, 19, 22]. According to surface temperature data collected at the meteorological station in the sampling area by scholars [33], they observed that, in the past ten years, the average temperature in Northern Shaanxi of the Loess Plateau has changed from −20°C to 20°C. Hence, the FT
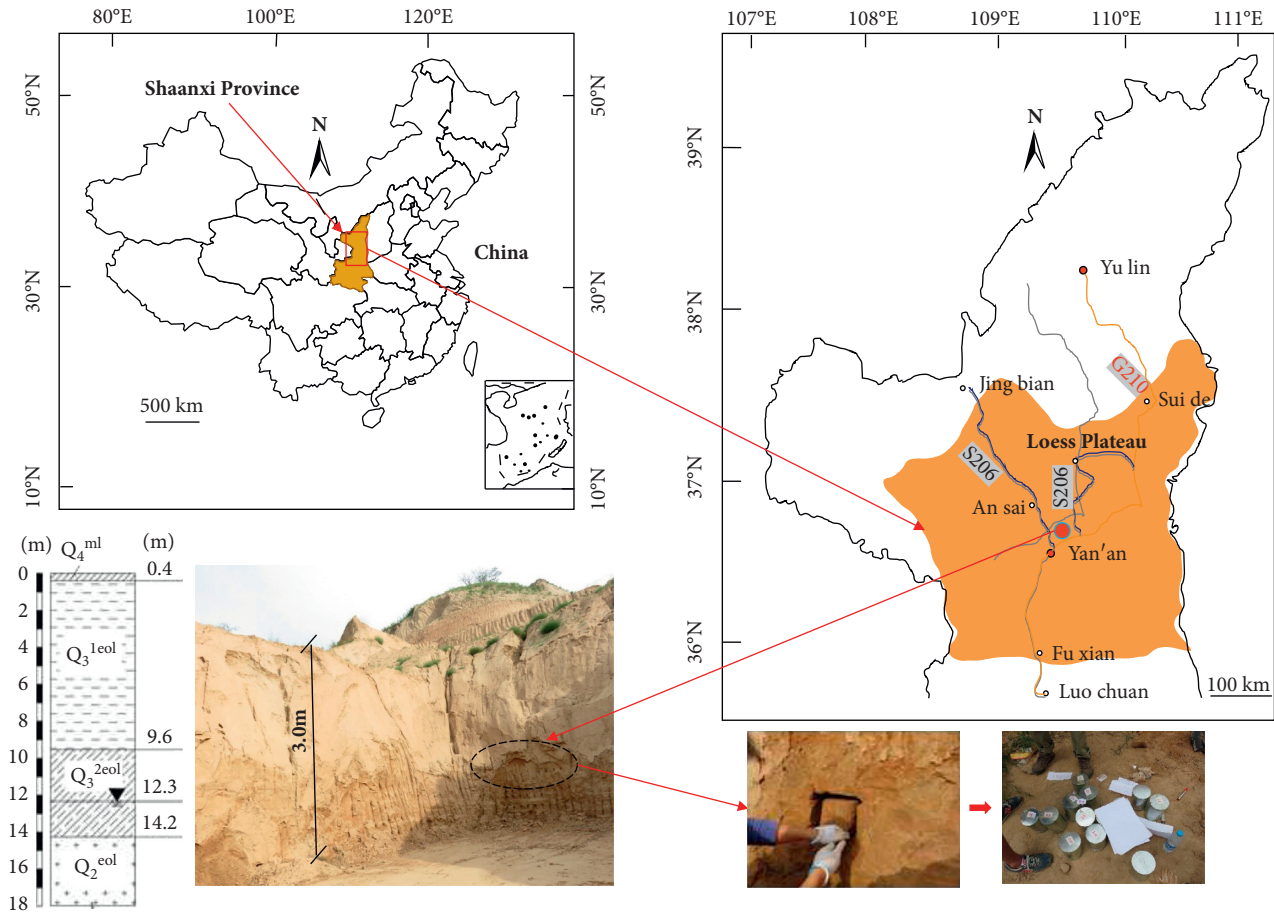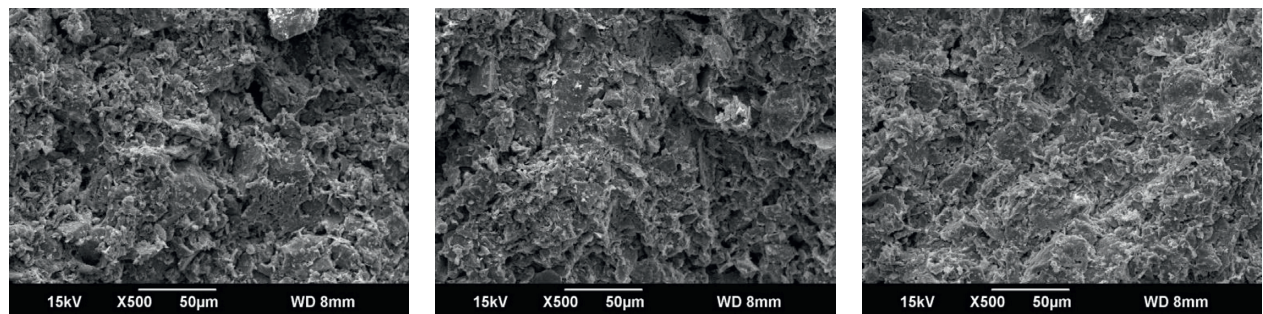
FIGURE 1: Sampling site at Yan'an, Shaanxi Province, China.

TABLE 1: Basic physical properties of the loess samples.

Natural water content (%)	Natural density	Void ratio	Liquid limit (%)	Plastic limit (%)	Specific gravity	Particle size distribution			
						Sand (>0.075 mm) (%)	Silt (0.075~0.05 mm) (%)	Clay (0.005~0.002 mm) (%)	Colloidal particles (<0.002 mm) (%)
14.80	1.49 g/cm^3	1.05	31.20	20.60	2.71	16.35	53.15	15.76	14.74

FIGURE 2: SEM images of the samples: (a) group a; (b) group b; (c) group c.
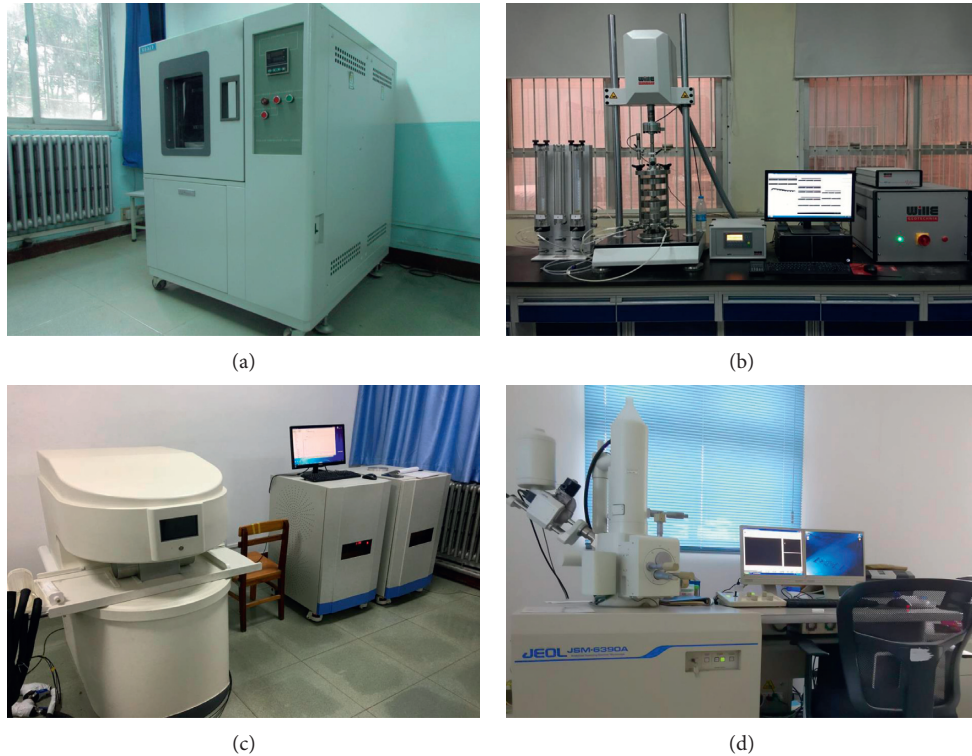
(a)

(b)

(c)

(d)

FIGURE 3: Photographs of the apparatus used in the tests: (a) high/low temperature test chamber; (b) triaxial testing machine; (c) nuclear magnetic resonance equipment; (d) scanning electron microscope.

scheme of freezing at −20°C and thawing at 20°C was appropriate. For the freezing or thawing time of a single FTC, no recognized standard has been proposed, and it is usually set comprehensively based on research motivation, test conditions, and engineering background. In previous studies, when a closed (no water supplement) FT scheme was adopted, it was generally considered that the response of the soil structure and deformation characteristics to the FT effect had reached a stable level after continuous freezing (or thawing) for 12 h [15]. Therefore, one FT cycle was determined to comprise −20°C for 12 h and then 20°C for 12 h. The specific numbers of FT cycles tested were 0, 1, 3, 6, 10, and 15 [17]. It is needed to explain that the greatest deterioration in soil structure may occur in the initial FT cycles, and after ten cycles, a new dynamic equilibrium generally appears [16, 19]. Based on this, an upper limit of 15 and specific numbers (0, 1, 3, 6, 10, and 15) of cycles were set.

2.2.2. Measurement of Sample Water Migration. Numerous studies have reported that, to analyze the influence of freeze-thaw cycles on the mechanical properties of soil, attention must be paid to water migration [8, 17, 21]. Therefore, water migration (the cylindrical sample was circularly cut into five equal parts in the radial direction and dried separately, see Figure 4) in thawed samples were evaluated.

2.2.3. Triaxial Shear Tests. The specimens used for triaxial strength tests consisted of two groups with initial water contents of 18% and 22%. Each group contained 12
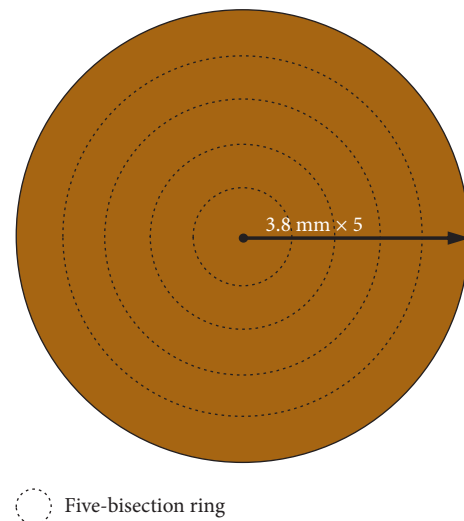

3.8 mm × 5

⋯⋯ Five-bisection ring

FIGURE 4: Schematic diagram of tests for sample dimensional change and water migration.

specimens. Taking into account that consolidation will affect the damage caused by FTC, in addition, the poorly permeable loess is difficult to drain in reality [17, 35], the unconsolidated undrained (UU) scheme is adopted in our triaxial strength test. Four triaxial samples with the same water content and number of FT cycles were selected for UU triaxial shear tests. A triaxial test apparatus (LO7010/5DYN, Wille-Geotechnik, Germany; Figure 3(b)) was employed to apply various confining pressures (50, 100, 150, and 200 kPa,

as per the in situ condition). Triaxial shear tests were conducted at a rate of 0.1 mm/min and terminated when the axial strain reached 16% (according to China Soil Test Standard [34]).

2.2.4. NMR Tests. After FT treatment, the samples were divided into six groups; according to the number of FT cycles, they had received and subjected to NMR testing. Each group contained samples of two water contents (18% and 22%), which were saturated with distilled water in a vacuum. Then, an NMR analyzer (Macromr12-150h-i, Niumag Technology, China; Figure 3(c)) was used to measure the evolution and distribution of pores in the soil samples. It is worth noting that ferromagnetic substances interfere with the magnetic field of the NMR test instrument and affect the test accuracy [29]. Hence, the specimens required for NMR were compacted with correspondingly sized polyvinyl chloride (PVC) sleeves instead of the traditional steel soil sample molds. Moreover, it should be mentioned that the saturated sample used here conforms to the principle of NMR measuring pore structure in porous media, that is, only pores filled with hydrogenous fluid can be inspected [31]. The specific principles and methods are as follows.

When the porous materials are completely filled with water, its NMR transverse relaxation time (T_2) has a good correspondence with the water-imparting pore size (d) [36–38], as expressed by the following equation:

$$\frac{1}{T_2} = \rho_2 \left(\frac{S}{V}\right)_{pore} = \rho_2 \left(\frac{2F_S}{d}\right), \quad (1)$$

where ρ_2 represents the transverse relaxation rate (which, for natural porous media, is 0–$10\,\mu m \cdot s^{-1}$ and for loess is $3.0\,\mu m \cdot s^{-1}$ [39, 40]), S/V stands for the ratio of the surface area to the volume of the pores in the sample, and F_S is the pore shape factor (when using a cylindrical model for approximate analysis, $F_S = 2$ [29, 31]). Generally, the loess pores are divided into four categories according to their average equivalent diameters [21]; i.e., micropores ($d < 5\,\mu m$), small pores ($5^\circ \leq^\circ d < 10\,\mu m$), mesopores ($10^\circ \leq^\circ d \leq 20\,\mu m$), and macropores ($d > 20\,\mu m$).

2.2.5. SEM Tests. Six groups of samples were observed by SEM, which had experienced 0, 1, 3, 6, 10, or 15 FT cycles. Each FT-cycle group contained samples of two water contents. Each sample was dried by natural air (25°C, RH 50%, 14 d), trimmed, and a relatively flat fresh section selected from it. This was processed into a 1 cm³ cubic specimen and sprayed with Pt to enhance its conductivity. Micrographs were obtained by SEM (JSM-6390A, JEOL, Japan; Figure 3(d)) to observe the microstructural characteristics of each specimen. The particle and pore parameters contained in the micrographs were measured by a particles (pores) and cracks analysis system [26, 30, 41]. The particle orientation frequency and fractal dimension of the pore network were accurately estimated. The details are as follows.

Referring to the parameter extraction methods described in the published literature [30, 41], PCAS software was utilized to segment the 500x magnification SEM images, as shown in Figure 5(a). We then extracted geometric information relevant to pores and particles through the automatic tracking function (Figure 5(b)).

The degree of arrangement of soil granular structural elements after FTC can be described in terms of the soil particle directional frequency $F_i(\alpha)$, which is defined as [42]

$$F_i(\alpha) = \left(\frac{m_i}{M}\right) \times 100\%, \quad (2)$$

where m_i represents the number of particles in a certain azimuthal region, M is the total particle number, and α denotes the angle of each location after dividing the range $0°$–$180°$ into n equal parts; hence, $\alpha = 180°/n$. Here, $n = 12$ and $\alpha = 15°$. In this study, we assumed that the directional distribution of particles in the range of $0°$–$360°$ was symmetrical.

Fractal dimensions can effectively characterize the tortuosity or complexity of a soil pore network. It is generally believed that there are three fractal dimensions of a soil structure, namely, the mass, spectrum, and surface [43]. Among them, the mass fractal dimension (also called the box-counting fractal dimension [44]) is often used to describe the space-filling ability of an object [45]. Our study evaluated the change in the mass fractal dimension of the pore network of natural loess in an FT environment through the box-counting method:

$$N(\varepsilon) = \left(\frac{1}{\varepsilon}\right)^{D_{m\_box}}. \quad (3)$$

Here, D represents the fractal dimension of the pore network. A series of recorded data pairs are plotted in the log $(1/\varepsilon)$ against log $\{N(\varepsilon)\}$ coordinate system, and the fractal dimension is estimated by the slope of the curve.

3. Results

3.1. Effect of FT Cycles on Water Migration. The characteristics of the water content relative change (the ratio of the increment of water content measured in the thawed specimen after a certain number of FT cycles to the initially water content of the specimen before cycles) along the radial direction after FTC of the samples are shown in Figure 6. From Figure 6(a), within the first three cycles, the water redistribution in various samples shows almost consistent, with all having greater water contents in the surface layer than inside. This means that the water that migrated to the surface due to freezing could not fully migrate back during the melting process. Taking the $w = 18\%$ sample as an example, the increase in surface water content occurred in the first 6 FT cycles, and the water content at each location no longer changed significantly after 10 cycles (Figure 6(b)).

3.2. Effect of FT Cycles on the Mechanical Behavior of Samples

3.2.1. Stress-Strain Curves. Figure 7 shows the stress-strain curves of the various specimens after several FT cycles. From Figure 7(a), especially when not subject to FTC, the water
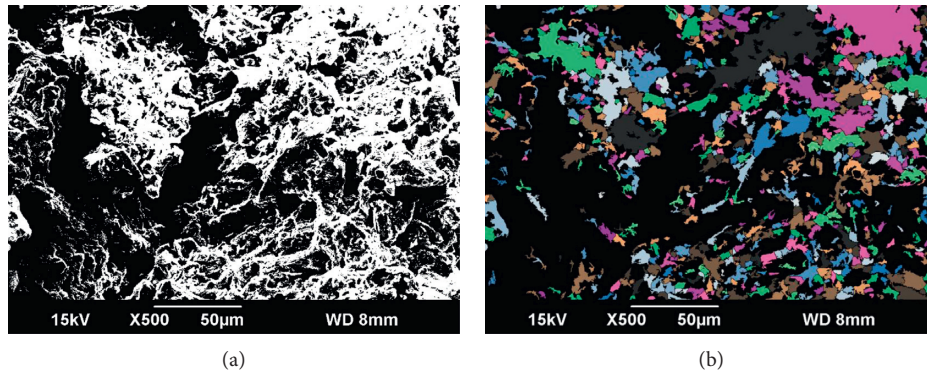
(a)   (b)

FIGURE 5: SEM image processing: (a) binary processing; (b) microstructural identification.

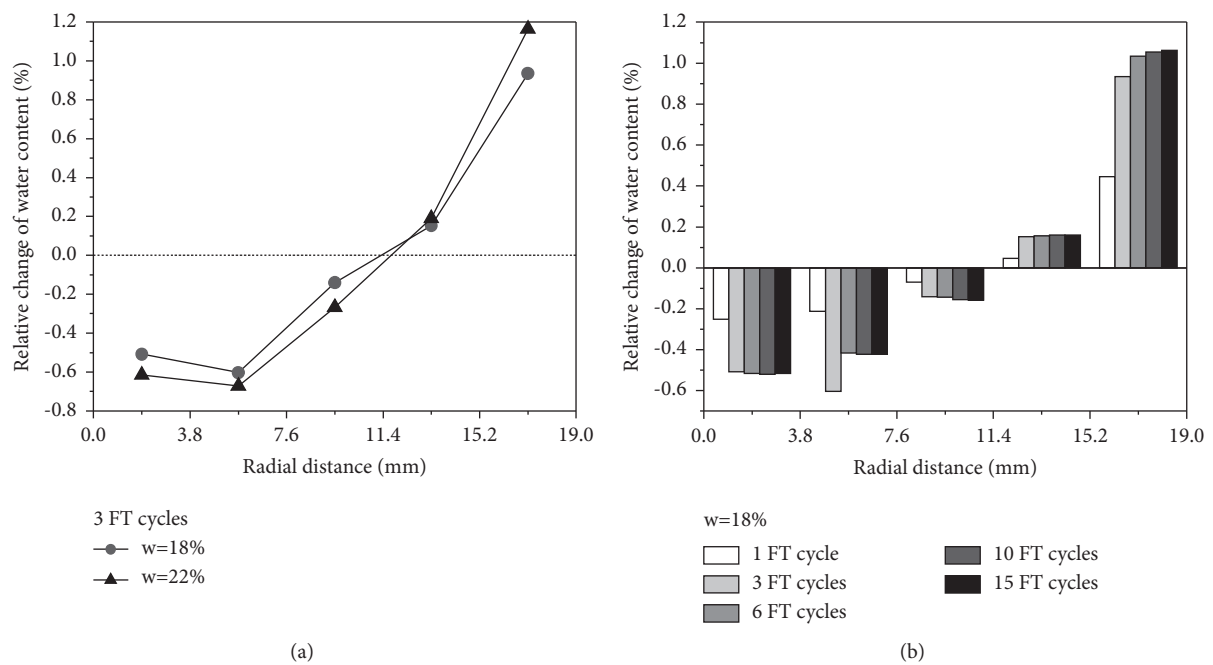(a)   (b)

FIGURE 6: Radial water migration characteristics of samples with FTC: (a) influence of water content; (b) influence of FT cycles.

contents of samples increased and the stress-strain curves evolved from a strong strain-hardening type to a weak strain-hardening type (strain-hardening, i.e., the deviator stress always increases with the increase of the axial strain [15, 19]). After six FT cycles, the stress-strain curves of each sample showed a strain-hardening trend and the hardening amplitude did not change much with increases in water content (Figure 7(a)). These results indicate that the shape of the stress-strain curves of loess is more controlled by the initial water content than by the FT cycles. When the confining pressure level and water content were held constant ($\sigma_3 = 100\,kPa$ and $w = 18\%$), while the number of FT cycles increased (Figure 7(b)), the shape of the stress-strain curves was roughly similar under different confining pressures; however, their peak values of deviator stress decrease obviously. This means that FTC has limited influence on the shape of the loess stress-strain curve, but it has a significant attenuation effect on the peak deviatoric stress of the soil.

Moreover, from Figure 7(c), when the water content and FTC were held constant ($w = 18\%$, six cycles), with decreases in confining pressure, the stress-strain curve gradually transitioned from a strong strain-hardening type to a weak strain-hardening type and, finally, approached an ideal plastic type. It can be concluded that shape of the stress-strain curve of soil is significantly controlled by the confining pressures.

3.2.2. Failure Strength. We further examined the characteristics of the obtained stress-strain curves and recorded the maximum deviator stress of each curve. As per [46–48], for the fully-hardened curve, the deviator stress at which the sample strain reached 15% was taken as the failure strength. The curves of failure strength evolution with FTC for each sample in 100 kPa confining pressure are collated in Figure 8. Generally, the failure strength of the various samples
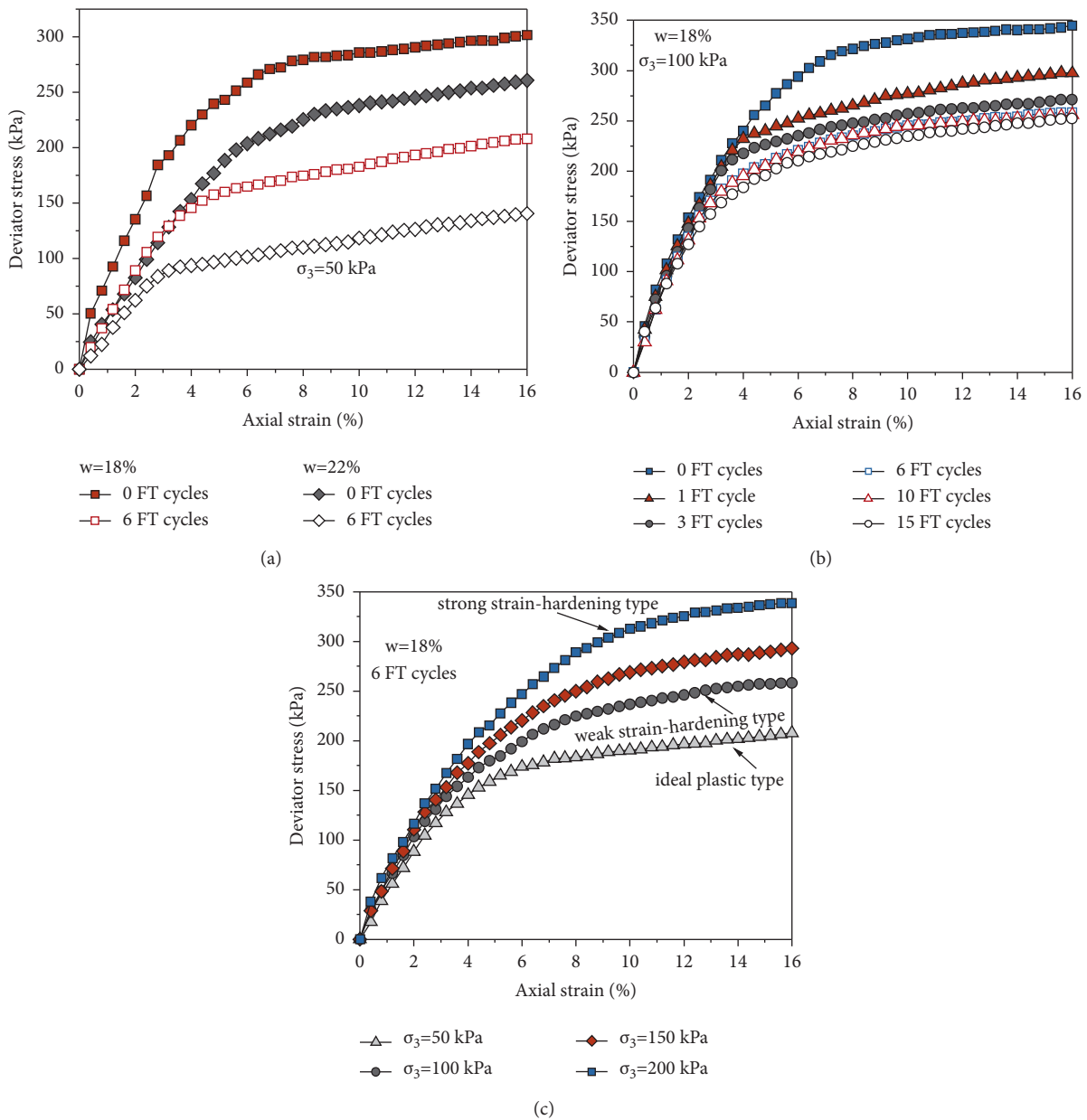
(a)

(b)

(c)

FIGURE 7: Stress-strain curves of samples under FT cycling: (a) influences of water content; (b) influences of FT cycles; (c) influences of confining pressure.

deteriorated significantly with FTC. Over all FT cycles, the general trends in the failure strength curves for various samples were similar and can be roughly divided into the following three stages: (i) sudden decrease, (ii) slow decrease, and (iii) equilibrium. Quantitative analysis shows that, after all FT cycles, the losses in failure strength (difference from the initial value divided by the initial value) of samples with initial water contents of 18% and 22% were 26.47% and 23.30%, respectively. Furthermore, it should be noted that, in the sample with the high-water content ($w = 22\%$), after undergoing three FT cycles, the failure strength decayed to a stable level, while the samples with less water required six FT cycles to reach stability. It can be concluded that, in the initial three FT cycles, the

deterioration in failure strength was more significant with increases in the initial water content. However, during the entire FTC process, the attenuation of the failure strength of the samples with low initial water content is more significant.

3.2.3. Shear Strength Parameters. Based on the total stress method [30, 34], the variation of shear strength parameters with freeze-thaw cycles is obtained, as shown in Figure 9. As the number of FT cycles increased, the cohesion of the specimens decreased exponentially. For the low-water content samples ($w = 18\%$), the attenuation of cohesion was embodied in the first six FT cycles, while the high-water
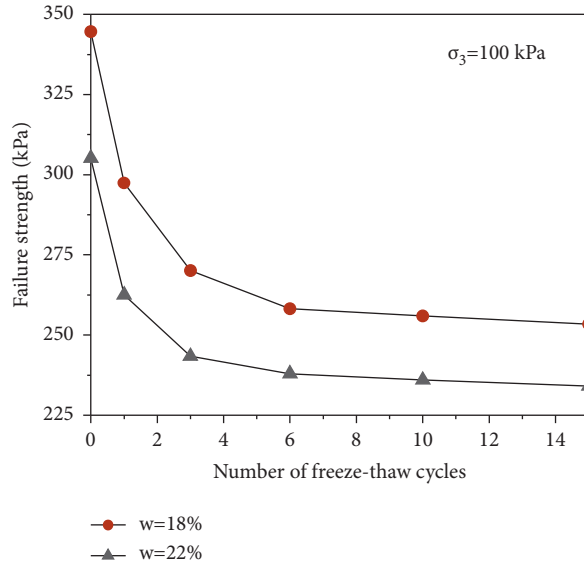
FIGURE 8: Evolution in the failure strength of samples with FTC ($\sigma_3 = 100$ kPa).
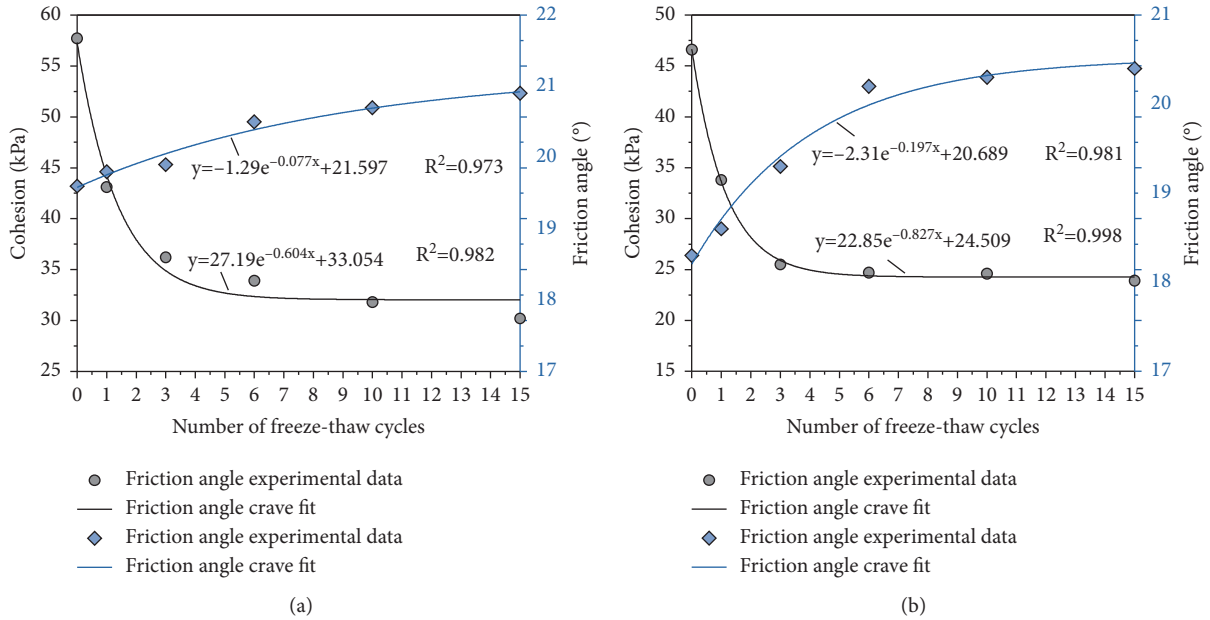

FIGURE 9: Evolution in the cohesion and friction angle of specimens with FTC; (a) $w = 18\%$; (b) $w = 22\%$.

content samples ($w = 22\%$) only required three cycles. Additionally, in specimens with higher initial water content ($w = 22\%$), the overall cohesion attenuation amplitude (47.21%) was weaker than in specimens with low water content ($w = 18\%$ and 49.64%). However, in the initial three FT cycles, the sample with high water content ($w = 22\%$) had a loss of cohesion of up to 45.28%, while the sample with low water content ($w = 18\%$) had a loss of cohesion of 34.85%. In terms of internal friction angle, there was a slight strengthening trend over the whole cycling process, but the increase amplitude generally remained <3°. This implies that, in the FT environment, cohesion is lost more rapidly at higher soil water contents and fewer FT cycles are required for the strength to decay to stability. This trend is consistent

with the abovementioned trend in failure strength deterioration. Hence, it can be speculated that the decrease in the failure strength of loess is mainly due to the loss of cohesion, with the change in the internal friction angle being a secondary factor.

3.3. Effect of FT Cycles on the Microstructural Damage of Samples

3.3.1. NMR Test Results. NMR tests were performed on specimens after different numbers of FT cycles. This obtained the relationship between the amount of pore water inside the specimens (NMR signal amplitude) and the

number of cycles. The test results for the specimen with an initial water content $w = 18\%$ are clearly plotted in Figure 10. The T_2 distribution curves of the specimen after different numbers of cycles show multimodality, with one main peak and two secondary peaks. As the number of FT cycles increased, the main and secondary peaks enhanced in intensity. Nonetheless, the main peak increased much more than the secondary peak. Furthermore, there were two significant upward shifts in the main peak; the first in the sixth cycle and the other in the tenth. The amplitude of a sample's NMR signal is proportional to the pore volume [29, 31]. Based on this, further analysis showed that the pore content increased most significantly during cycles 3–6, less so in cycles 1–3, and least during 6–10 FT cycles (Figure 11).

Figure 12 shows the pore size distribution of the specimen with an initial water content $w = 18\%$. Overall, with increasing numbers of FT cycles, the volumes of pores of each size show different degrees of variation during the initial stages of FTC and then enter a dynamic stabilization trend. Among them, the small pores and macropores exhibit increasing trends, and the macropore volume increases most. The mesopores and micropores show decreasing trends, with mesopores decreasing more; however, the volumes of mesopores and small pores are always highest. This seems to indicate that when a specimen is subjected to FTC, the internal micro- and small-sized pores are continuously converted to medium- and macro-sized pores, the internal penetration fissures increase in size, and specimen damage increases continuously. However, the soil pores tend toward a mutual feedback equilibrium state after a certain number of FT cycles. Similar findings have also been reported in other studies, most of which used CT or MIP [19–21, 41, 46].

3.3.2. SEM Test Results. To comprehensively discern the microstructural variations occurring in soil samples with FTC, representative SEM micrographs ($w = 18\%$ and $w = 22\%$) at 1000x magnification were inspected (Figure 13 and 14). The skeleton structure of the natural specimens (i.e., before FTC) was mainly embedded and bridge-shaped, with mostly face-to-face contacts that were relatively firm. After six FT cycles, the morphology of the soil particles became significantly fragmented with mostly edge-to-face or point-to-face intergranular contact forms arranged in the form of overhead structures into wider through-pores. By comparison, with ten FT cycles, the particle morphology became increasingly fragmented and stacked disorderedly around other particles and pores. The soil fabric was altered significantly, with few soil particles still having cement between them, and the connections between particles were mostly point-to-edge or point-to-point. Furthermore, after ten FT cycles, the total number of pores in the field of view increased and initial structural degradation was observed. The soil particles were arranged loosely, and the contact forms were mostly point-to-point. Comparing Figures 13 and 14, it can be seen that the initial structure of the low water content sample was stronger. That is, the contours of the particles and pores are more complete. Especially, without freezing
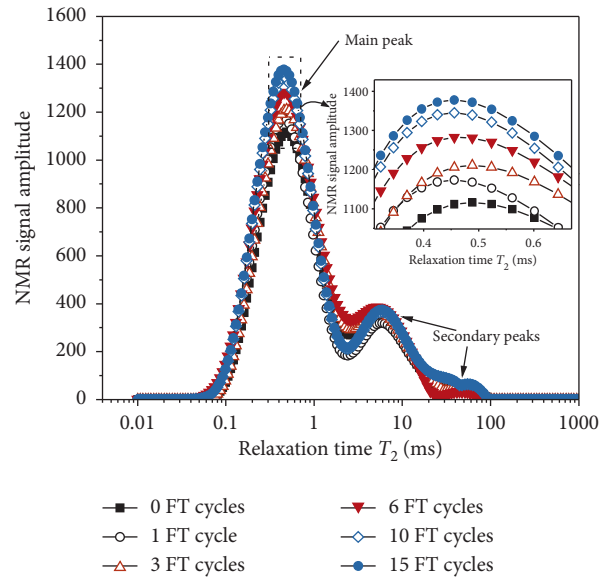

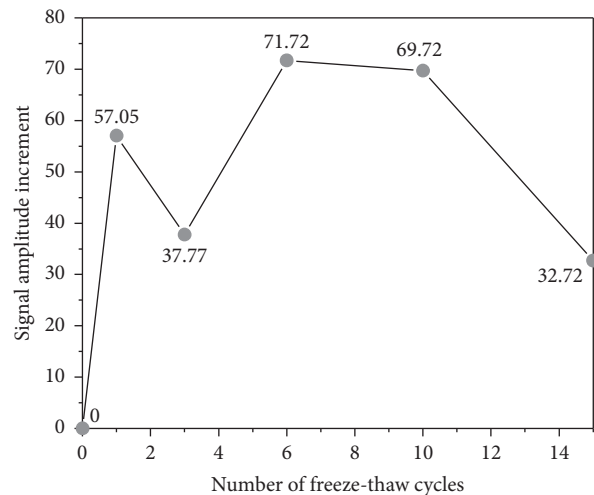FIGURE 10: T_2 hydrogen spectrum of a specimen ($w = 18\%$) after FT cycling.

FIGURE 11: Nuclear magnetic signal incremental distribution of a sample ($w = 18\%$) in an FT environment.

and thawing, the boundaries between particles and pores are vivid. For samples with high water content, even in the natural state, the proportion of broken particles in the field of view is relatively high, and the boundaries between particles and holes are relatively blurred. These observations imply that samples with high water content have lower initial structural strength and require less frost-heave stress and water migration potential to degrade.

Based on equation (2) and the extracted geometric parameters of the particles, a rose diagram of the directional frequency of each group of specimens was calculated, as depicted in Figure 15. With increasing FT cycles, the particle directional frequency of specimens decreased and homogenized at all angles. In the natural state (i.e., before FTC), the directional frequency of the soil particles was in a high-
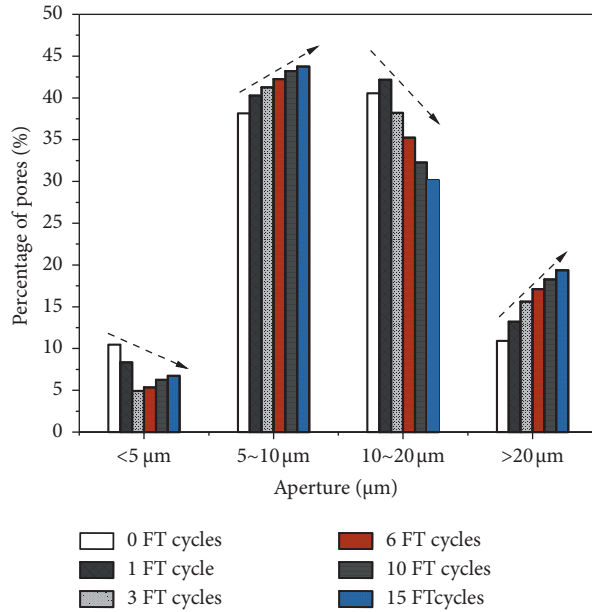
FIGURE 12: Pore size distributions of the specimens ($w = 18\%$) after FT cycling.
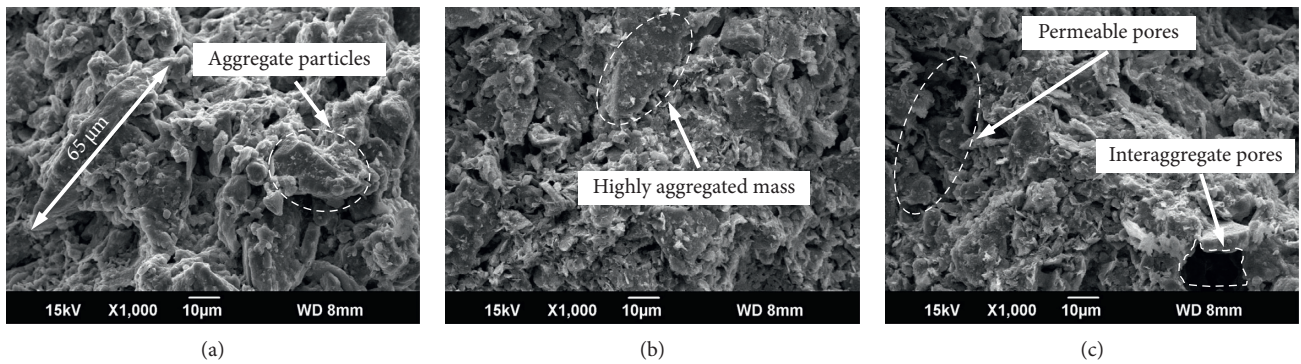

FIGURE 13: Photographs of the microstructure of a sample ($w = 18\%$) after (a) 0; (b) 6; (c) 10 FT cycles.
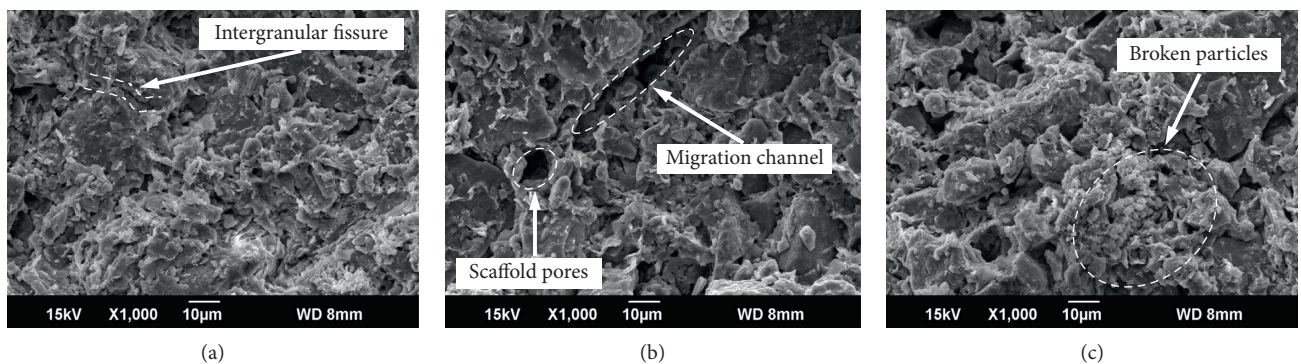

FIGURE 14: Photographs of the microstructure of a sample ($w = 22\%$) after (a) 0; (b) 6; (c) 10 FT cycles.

frequency range and, after six cycles, transformed into a relatively small and uniform state. Interestingly, the content of particles near certain polar angles (i.e., 0°, 90°, 180°, and 270°) showed a negative trend, which also seems to indicate that FTC will cause particle-oriented "depolarization" effects (as defined by Hattab and Fleureau [49]). Comparing Figure 15(a) and 15(b), it can be seen that the increase in soil water content has a certain influence on particle orientation
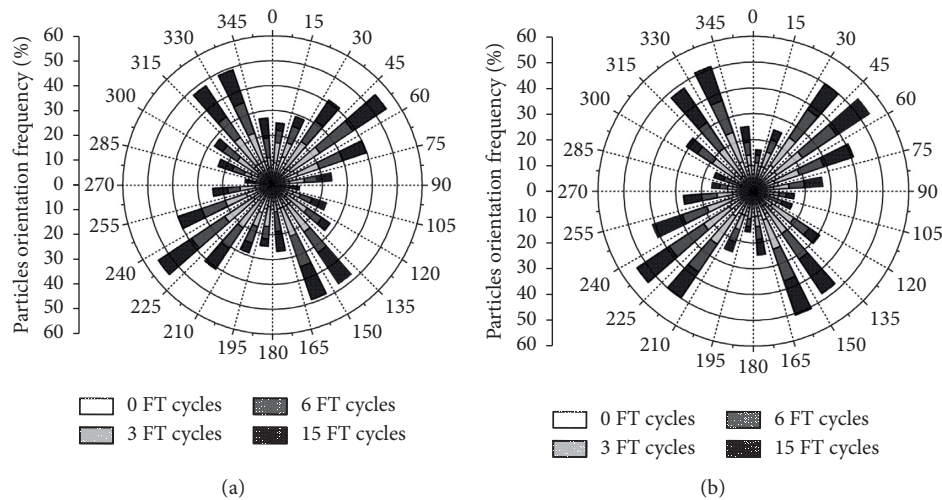
FIGURE 15: Rose diagram of the particle orientation frequency distribution of samples subjected to FT cycling: (a) $w = 18\%$ and (b) $w = 22\%$.

characteristics in a FT environment. It can be observed that the particle distributions in the dominant intervals ($30°–90°$, $120°–165°$, $210°–255°$, and $300°–345°$) are higher than those in low water content samples, and the distributions in the polar angle region are lower. This is probably because samples with higher water contents have more significant particle aggregation and dispersion behavior under FTC.

Based on equation (3) and the measured pore geometry parameters, we calculated the mass fractal dimension distribution of the pore network after FTC in each group of samples (Figure 16). It shows that the fractal dimensions increased with the number of FT cycles and always fluctuated. It can be seen from Figure 16 that the mass fractal dimension range of the natural loess pore network is basically 2.56 to 2.81 for FT environments. The literature [50] reports that the pore network mass fractal dimension of silty clay loam varies from 2.81 to 2.86 over six FT cycles. In addition, it is worth noting that the mass fractal dimension of the pore network continued to increase with FTC. This increase was embodied within the first three to six FT cycles. Subsequently, the mass fractal dimension tended toward equilibrium, which implies that, with increasing FTC, the degree of irregularity of the pore network continues to increase. Besides, when the frost heaving potential generated by the FTC weakens toward a certain critical value, the pore complication process is suppressed and a corresponding transition to an equilibrium state occurs. Indeed, it was also found that, under the same number of FT cycles, samples with a high initial water content had a higher final mass fractal dimension of the pore network, and the number of cycles required to increase to equilibrium was fewer.

4. Discussion

4.1. Evolution Mechanism of Loess Apparent Physical Properties Subjected to FTC. The complete FT process of soil involves an internal and external temperature difference. When freezing, the outer layer of the sample freezes first, namely, the temperature of the outer layer is lower than the
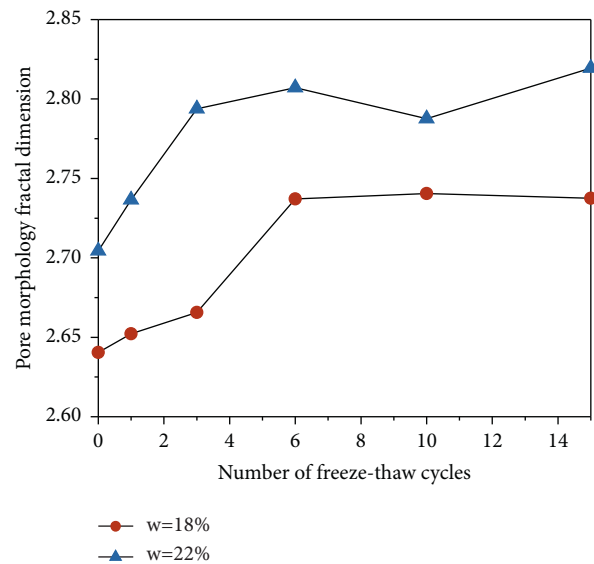

FIGURE 16: Mass fractal dimension of the soil pore network with FT cycling.

inside, causing the moisture inside the soil to migrate to the surface. The opposite is true when thawing, but the water that has migrated to the surface of the soil cannot be completely returned. It is generally believed that the moisture in the soil has a tendency to migrate to the freezing front under FT conditions [25, 51]. In other words, the amount of water migration is related to the temperature gradient and residence time of the freezing front at that location. Then, combined with the radial water content distributions of the tested samples (Figure 6), it can be determined that when the temperature gradient is constant, the greater increment of the water migration of the sample surface is associated with the longer residence time of freezing front at that location (i.e., a more slowly advancing freezing front). Another potential explanation is that the water migration potential in the soil depends on the temperature gradient, which is inversely proportional to the heat

conduction distance [13, 33]. The side area of the cylindrical samples used in the study was much larger than that of the top and bottom areas. In a closed FT environment, the radial distribution of moisture in a sample is much more uneven than that in the axial direction. Moreover, the moisture on the surface of a sample cannot fully migrate back to the interior during the thawing process, and the water content of the surface increases after several FT cycles (Figure 6).

4.2. Mechanism of Shear Strength Degradation of Loess Subjected to FTC. The main reason for the attenuation in the failure strength of specimens was the repeated frost-heave stress and migration potential caused by FTC [8, 21]. The frost-heave stress has a squeezing effect on the microstructure of soil, which weakens the cementation between particles upon which soil cohesion is largely dependent [17, 29] and significantly reduces cohesion. A similar point was made in an investigation [52], which reported that soil cohesion is attenuated more rapidly at higher water contents under FTC. Our results similarly indicate that samples with higher water content ($w = 22\%$) required fewer FT cycles (three cycles) for their cohesion to drop to a plateau. Based on this, it can be further speculated that samples with high initial water contents have poor structural strength and relatively low initial cohesion; hence, fewer FT cycles are required to decay to stability. Therefore, in seasonally frozen loess areas, attention should be paid to soil drainage to reduce the soil water content and limit deterioration in soil strength due to FTC. Secondly, in seasonally frozen soil areas of the Loess Plateau, the mechanical index of soil after ten FT cycles may be considered the reference value for engineering design. In addition, during FTC, the internal aggregates of soil are continuously broken and metastable particles with more contact points (improved interlocking properties) are formed after being interspersed (the expansion of the water as it becomes ice). Meanwhile, the migration of water caused by the migration potential scours the surface (decreased antislipping properties) of the soil particles. Due to the friction angle mainly represents the antislipping and interlocking properties between the soil particles [29, 30]. The internal friction angle shows a slight increase and tends to equilibrium under these two mechanisms (Figure 9).

4.3. Mechanism of Microstructural Damage of Loess Subjected to FTC. The macroscopic strength of loess is governed by microstructure characteristics [30, 38, 41]. Under the action of FTC, the water inside soil freezes into ice and the soil volume tends to expand (especially when the soil moisture is high, the volume of ice crystals will be larger than the critical expansion space inside the soil), which has a destructive effect on the soil's original skeleton [53]. The ice lens causes the pores to expand or interpenetrate and evolve into slightly larger pores. This deduction is supported by the NMR test results. After several FT cycles, the T_2 hydrogen spectrum shifted significantly upward and shifted to the right, which means that the content and size of the pores increased (Figure 15). Similar behavior was observed by Zhou and Tang [54] in a study of muddy soil via MIP, which showed

that most of the pores turned into macropores and micropores at lower temperatures ($<-20°C$). Under the action of repeated FTC, the freezing-expansion and melting-shrinkage of soil particles become irreversible. Both cause detachment of the large skeleton aggregates, which have a complicated arrangement (Figures 13 and 14). This promotes the migration of capillary water and enhances the scouring effect on the edges of particles and the inner walls of pores. This effect directly causes particles near the polar angle to rotate (Figure 15), the fractal dimension of pore network to fluctuate slightly in the first FT cycles (Figure 16), and the content of pores to increase (Figure 10). In subsequent FTC, the destruction of the soil skeleton by the ice lens reaches a bottleneck (in a closed system, no water is supplied), although the agglomerating effect of soil particles is more marked. Simultaneously, some loose particles become more sensitive and rapidly interpenetrating, which makes the pore morphology more complex and increases the fractal dimensions of pore network (Figure 16). Combining the NMR and SEM results, it is easy to see that, as the volume of macropores increases, the fractal dimension of the pore network increases slightly. These findings corroborate those of Peyton et al. [55] and Luo et al. [56], who both reported a positive correlation between macropore volume and fractal dimension of the pore network in agricultural soils based on CT scanning.

The macroscopic mechanical properties and microstructural evolution mechanisms of loess subject to FTC are complex and are a hotspot of research into soil mechanics problems in cold regions. Some studies have employed MIP to reveal the soil pore evolution mechanism [20, 39, 57, 58]. The present study quantitatively used low-disturbance observations (NMR and SEM) to explore the evolutions in soil mechanical properties and microstructure under FT conditions. The microstructural evolution process in loess samples in an FT environment was abstracted from Figure 13 to create Figure 17. Combined with the above test results, the general mechanism of deterioration in the mechanical properties of loess in an FT environment is summarized as follows.

In an FT environment, repeated frost-heave stress and migration potential are generated in the soil. Among them, frost-heave stress extrusion destroys the interparticle coupling effect, causing some unstable particles to gradually exfoliate and causing interparticle distances to increase. Meanwhile, water migration caused by a temperature gradient causes the finer granules in the soil to penetrate the larger pores (Figure 11). Further, the orientation of the particles becomes uneven, and the fractal dimension of the pore network also increases (Figure 16). In a continuously FTC environment, soil cohesion exhibits a distinct attenuation trend and soil strength characteristics are gradually degraded. In summary, a dialectical analysis of the potential relationship between macroscale and microscale effects suggests that the macroscopic degradation of soil is an external manifestation of accumulated internal microstructural fatigue. Hence, irreversible internal microstructural damage is the potential mechanism of macroscopic degradation in soil.
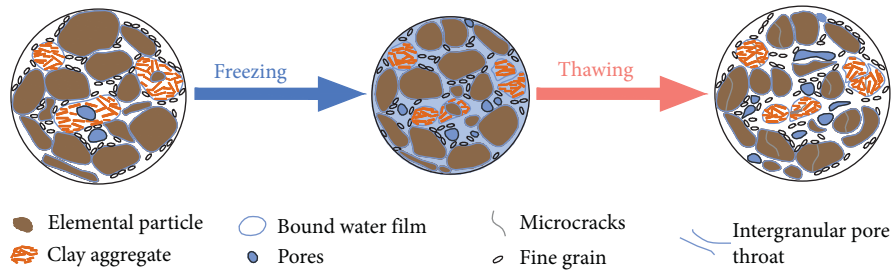
FIGURE 17: Schematic diagram of the microstructural evolution of loess with FT cycling.

5. Conclusions

In the present study, FT tests were performed on intact loess specimens with different water contents. The specimens were then tested by triaxial apparatus, NMR, and SEM. The potential relationships between FTC and soil physical-mechanical behavior and microstructural characteristics and their mechanisms were then discussed. The following conclusions are drawn.

(1) The FTC has a significant attenuation effect on the peak deviatoric stress of loess, but it has limited influence on the shape of the stress-strain curve. Compared with the FTC, the confining pressure has a more significant influence on the shape of the loess stress-strain curve.

(2) Deterioration in soil strength mainly occurred during the first six FT cycles and became balanced after ten cycles. The lower the soil water content, the greater the loss in failure strength caused over the entire FT process; however, during the initial FTC (first three cycles), samples with higher water contents had more severe losses of failure strength. The cohesion of natural loess decayed exponentially with increases in FTC but stabilized after 3–6 cycles. The sample with low water content ($w = 18\%$) had a more significant loss of cohesive force (49.64%) and required more FTC (six cycles) for attenuation to equilibrium than the sample with high water content ($w = 22\%$). The internal friction angle was slightly strengthened with increases in FT cycles (by about 2°).

(3) Under FTC, the T_2 hydrogen spectra of the soil samples showed a multimodal distribution. The main peaks showed two significant upward shifts after 6 and 10 cycles, respectively, and then stabilized. That is, the increase in sample pore volume mainly occurred during the first ten cycles. With increasing FTC, the finer pores gradually evolved into slightly larger pores and the soil pore volume and size increased. Among them, the volumes of macropores and small pores increased, with that of macropores being more conspicuous. The volumes of mesopores and micropores decreased, with that of mesopores being more significant.

(4) As the number of FT cycles increases, the original embedded and bridge structures of the soil collapse and the intergranular connection mode gradually changes from face-to-face to point-face or point-edge. Under FTC, the orientation frequency of particles is depolarized; that is, the overall soil structure is isotropic and the worst orientations are at the local polar angles of 0°, 90°, 180°, and 270°. For a given number of FT cycles, soil with higher water content has a greater increase in the pore network mass fractal dimension.

(5) Under the action of FTC, the water phase in loess changes repeatedly, causing fluctuations in the water migration potential and frost-heave stress that cause irreversible damage to the soil microstructure (pore coarsening, particle breakage, and cementation dissolution). This is the potential mechanism of strength reduction in loess.

Data Availability

The data used to support the findings of this study are available from the corresponding author upon request.

Conflicts of Interest

The authors declare that they have no conflicts of interest.

Acknowledgments

References

[1] C. D. F. Rogers, T. A. Dijkstra, and I. J. Smalley, "Hydro-consolidation and subsidence of loess: studies from China, Russia, north America and Europe," *Engineering Geology*, vol. 37, no. 2, pp. 83–113, 1994.

[2] K. Pye, "The nature, origin and accumulation of loess," *Quaternary Science Reviews*, vol. 14, no. 7-8, pp. 653–667, 1995.

[3] M. Pésci, "Loess is not just the accumulation of dust," *Quaternary International*, vol. 7-8, pp. 1–21, 1990.

[4] H. Lin, D. X. Lei, C. S. Zhang, Y. X. Wang, and Y. L. Zhao, "Deterioration of non-persistent rock joints: a focus on impact of freeze-thaw cycles," *International Journal of Rock Mechanics and Mining Sciences*, vol. 135, Article ID 104515, 13 pages, 2020.

[5] G. Wang, W. Ye, and Y. Lv, "Loess geoheritage and geohazard protective measures at Luochuan loess national geopark in NW China," *Geoheritage*, vol. 11, no. 3, pp. 1089–1100, 2019.

[6] S. H. Wang, Q. Z. Wang, J. Xu, and J. L. Ding, "Effect of freeze-thaw on freezing point and thermal conductivity of loess," *Arabian Journal of Geosciences*, vol. 13, Article ID 206, 15 pages, 2020.

[7] H. Lin, D. X. Lei, R. Yong, C. Jiang, and S. G. Du, "Analytical and numerical analysis for frost heaving stress distribution within rock joints under freezing and thawing cycles," *Environmental Earth Sciences*, vol. 79, Article ID 305, 17 pages, 2020.

[8] J. Qi, P. A. Vermeer, and G. Cheng, "A review of the influence of freeze-thaw cycles on soil geotechnical properties," *Permafrost and Periglacial Processes*, vol. 17, no. 3, pp. 245–252, 2006.

[9] J. Graham and V. C. S. Au, "Effects of freeze-thaw and softening on a natural clay at low stresses," *Canadian Geotechnical Journal*, vol. 22, no. 1, pp. 69–78, 1985.

[10] P. Viklander, "Permeability and volume changes in till due to cyclic freeze/thaw," *Canadian Geotechnical Journal*, vol. 35, no. 3, pp. 471–477, 1998.

[11] G. Beskow, "Soil freezing and frost heaving with special application to roads and railroads," *Swedish. Geological Survey Year Book*, vol. 26, no. 3, 1935.

[12] K. D. Eigenbrod, "Effects of cyclic freezing and thawing on volume changes and permeabilities of soft fine-gained soils," *Canadian Geotechnical Journal*, vol. 33, no. 4, pp. 529–537, 1996.

[13] T. Wang, P. Li, Z. Li et al., "The effects of freeze-thaw process on soil water migration in dam and slope farmland on the Loess Plateau, China," *The Science of the Total Environment*, vol. 666, pp. 721–730, 2019.

[14] S. Kawamura and S. Miura, "Rainfall-induced failures of volcanic slopes subjected to freezing and thawing," *Soils and Foundations*, vol. 53, no. 3, pp. 443–461, 2013.

[15] G.-y. Li, W. Ma, Y.-h. Mu, F. Wang, S.-z. Fan, and Y.-h. Wu, "Effects of freeze-thaw cycle on engineering properties of loess used as road fills in seasonally frozen ground regions, north China," *Journal of Mountain Science*, vol. 14, no. 2, pp. 356–368, 2017.

[16] D.-y. Wang, W. Ma, Y.-h. Niu, X.-x. Chang, and Z. Wen, "Effects of cyclic freezing and thawing on mechanical properties of Qinghai-Tibet clay," *Cold Regions Science and Technology*, vol. 48, no. 1, pp. 34–43, 2007.

[17] J. Xu, J. Ren, Z. Wang, S. Wang, and J. Yuan, "Strength behaviors and meso-structural characters of loess after freeze-thaw," *Cold Regions Science and Technology*, vol. 148, pp. 104–120, 2018.

[18] S. Leroueil, J. Tardif, M. Roy, P. L. Rochelle, and J.-M. Konrad, "Effects of frost on the mechanical behaviour of Champlain sea clays," *Canadian Geotechnical Journal*, vol. 28, no. 5, pp. 690–697, 1991.

[19] J. Xu, Y. F. Li, W. Lan, and S. H. Wang, "Shear strength and damage mechanism of saline intact loess after freeze-thaw cycling," *Cold Regions Science and Technology*, vol. 164, Article ID 102779, 14 pages, 2019.

[20] C. G. Yan, Z. Q. Zhang, and Y. L. Jing, "Characteristics of strength and pore distribution of lime-flyash loess under freeze-thaw cycles and dry-wet cycles," *Arabian Journal of Geosciences*, vol. 10, Article ID 544, 10 pages, 2017.

[21] W. Ye and C. Li, "The consequences of changes in the structure of loess as a result of cyclic freezing and thawing," *Bulletin of Engineering Geology and the Environment*, vol. 78, no. 3, pp. 2125–2138, 2019.

[22] P. Delage and G. Lefebvre, "Study of the structure of a sensitive Champlain clay and of its evolution during consolidation," *Canadian Geotechnical Journal*, vol. 21, no. 1, pp. 21–35, 1984.

[23] Z. Zhang, W. Ma, W. Feng, D. Xiao, and X. Hou, "Reconstruction of soil particle composition during freeze-thaw cycling: a review," *Pedosphere*, vol. 26, no. 2, pp. 167–179, 2016.

[24] W. Watkins, A. Casagrande, and S. Taber, "Discussion on frost heaving," *Process Highway Research board*, vol. 11, pp. 165–177, 1931.

[25] A. W. Rempel, J. S. Wettlaufer, and M. G. Worster, "Premelting dynamics in a continuum model of frost heave," *Journal of Fluid Mechanics*, vol. 498, pp. 227–244, 2004.

[26] C. Liu, B. Shi, J. Zhou, and C. Tang, "Quantification and characterization of microporosity by image processing, geometric measurement and statistical methods: application on SEM images of clay materials," *Applied Clay Science*, vol. 54, no. 1, pp. 97–106, 2011.

[27] K. Liu, W. P. Hu, C. Gao, and W. J. Ye, "Energy dissipation of an infinite damping beam supported by saturated poroelastic halfspace," *Physica Scripta*, vol. 96, Article ID 055220, 12 pages, 2021.

[28] Y. Lu, S. Liu, L. Weng, L. Wang, Z. Li, and L. Xu, "Fractal analysis of cracking in a clayey soil under freeze-thaw cycles," *Engineering Geology*, vol. 208, pp. 93–99, 2016.

[29] K. Liu, W. J. Ye, H. J. Gao, and Q. Dong, "Multi-scale effects of mechanical property degradation of expansive soils under drying-wetting environments," *Chinese Journal of Rock Mechanics and Engineering*, vol. 39, no. 10, pp. 2148–2159, 2020.

[30] J. Xu, Y. Li, S. Wang, Q. Wang, and J. Ding, "Shear strength and mesoscopic character of undisturbed loess with sodium sulfate after dry-wet cycling," *Bulletin of Engineering Geology and the Environment*, vol. 79, no. 3, pp. 1523–1541, 2020.

[31] F. Shi, C. Zhang, J. Zhang, X. Zhang, and J. Yao, "The changing pore size distribution of swelling and shrinking soil revealed by nuclear magnetic resonance relaxometry," *Journal of Soils and Sediments*, vol. 17, no. 1, pp. 61–69, 2017.

[32] C. Buchmann, M. Meyer, and G. E. Schaumann, "Characterization of wet aggregate stability of soils by H-NMR relaxometry," *Magnetic Resonance in Chemistry*, vol. 53, no. 9, pp. 694–703, 2015.

[33] J. Xu, Z.-q. Wang, J.-w. Ren, S.-h. Wang, and L. Jin, "Mechanism of slope failure in loess terrains during spring thawing," *Journal of Mountain Science*, vol. 15, no. 4, pp. 845–858, 2018.

[34] M. W. P. R. C., "Ministry of water resources of the people's Republic of China," *National Standards of the People's Republic of China: Standard for Geotechnical Testing Method (GB/T50123-2019)*, China Planning Press, Beijing, China, 2019.

[35] G. Spagnoli, D. Rubinos, H. Stanjek, T. Fernández-Steeger, M. Feinendegen, and R. Azzam, "Undrained shear strength of clays as modified by pH variations," *Bulletin of Engineering Geology and the Environment*, vol. 71, no. 1, pp. 135–148, 2012.

[36] J. Dong, H. Lyu, G. Xu, and C. He, "NMR-based study on soil pore structures affected by drying-wetting cycles," *Arabian Journal for Science and Engineering*, vol. 45, no. 5, pp. 4161–4169, 2020.

[37] S. Godefroy, J. P. Korb, M. Fleury, and R. G. Bryant, "Surface nuclear magnetic relaxation and dynamics of water and oil in

microporous media," *Physical Review A*, vol. 64, Article ID 021605, 13 pages, 2001.

[38] H. Lu, S. Xu, D. Li, and J. Li, "An experimental study of mineral and microstructure for undisturbed loess polluted by landfill leachate," *KSCE Journal of Civil Engineering*, vol. 22, no. 12, pp. 4891–4900, 2018.

[39] L. M. Anovitz and D. R. Cole, "Characterization and analysis of porosity and pore structures," *Reviews in Mineralogy and Geochemistry*, vol. 80, no. 1, pp. 61–164, 2015.

[40] F. Jaeger, E. Grohmann, and G. E. Schaumann, "^{1}H NMR relaxometry in natural humous soil samples: insights in microbial effects on relaxation time distributions," *Plant and Soil*, vol. 280, pp. 209–222, 2010.

[41] S. Wang, J. Ding, J. Xu, J. Ren, and Y. Yang, "Shear strength behavior of coarse-grained saline soils after freeze-thaw," *KSCE Journal of Civil Engineering*, vol. 23, no. 6, pp. 2437–2452, 2019.

[42] X. Xie, S. Qi, F. Zhao, and D. Wang, "Creep behavior and the microstructural evolution of loess-like soil from Xi'an area, China," *Engineering Geology*, vol. 236, pp. 43–59, 2018.

[43] A. N. Anderson, A. B. Mcbratney, and E. A. Fitzpatrick, "Soil mass, surface, and spectral fractal dimensions estimated from thin section photographs," *Soil Science Society of America Journal*, vol. 60, no. 4, pp. 962–969, 1996.

[44] D. Giménez, R. R. Allmaras, E. A. Nater, and D. R. Huggins, "Fractal dimensions for volume and surface of interaggregate pores - scale effects," *Geoderma*, vol. 77, no. 1, pp. 19–38, 1997.

[45] J. S. Perret, S. O. Prasher, and A. R. Kacimov, "Mass fractal dimension of soil macropores using computed tomography: from the box-counting to the cube-counting algorithm," *European Journal of Soil Science*, vol. 54, no. 3, pp. 569–579, 2003.

[46] A. S. T. M., *American Society of Testing Materials: Standard Test Methods for Unconsolidated Undrained Traixial Compression Test on Cohesive Soils (D2850-15)*, ASTM International, West Conshohocken, Pennsylvania, 2015.

[47] S. Y. Wang, R. Luna, and J. S. Yang, "Effect of plasticity on shear behavior of low-plasticity fine-grained soil," *Journal of Materials in Civil Engineering*, vol. 29, Article ID 04016228, 7 pages, 2017.

[48] W. Y. Zhang, A. B. Guo, and C. Lin, "Effects of cyclic freeze and thaw on engineering properties of compacted loess and lime-stabilized loess," *Journal of Materials in Civil Engineering*, vol. 29, Article ID 04019205, 12 pages, 2019.

[49] M. Hattab and J.-M. Fleureau, "Experimental study of kaolin particle orientation mechanism," *Géotechnique*, vol. 60, no. 5, pp. 323–331, 2010.

[50] T. Starkloff, M. Larsbo, J. Stolte, R. Hessel, and C. Ritsema, "Quantifying the impact of a succession of freezing-thawing cycles on the pore network of a silty clay loam and a loamy sand topsoil using X-ray tomography," *Catena*, vol. 156, pp. 365–374, 2017.

[51] R. W. Style and S. S. L. Peppin, "The kinetics of ice-lens growth in porous media," *Journal of Fluid Mechanics*, vol. 692, pp. 482–498, 2012.

[52] Y. Guo and W. Shan, "Monitoring and experiment on the effect of freeze-thaw on soil cutting slope stability," *Procedia Environmental Sciences*, vol. 10, pp. 1115–1121, 2011.

[53] Y. Zhang, A. E. Johnson, and D. J. White, "Freeze-thaw performance of cement and fly ash stabilized loess," *Transportation Geotechnics*, vol. 21, Article ID 100279, 10 pages, 2019.

[54] J. Zhou and Y. Tang, "Experimental inference on dual-porosity aggravation of soft clay after freeze-thaw by fractal and

probability analysis," *Cold Regions Science and Technology*, vol. 153, pp. 181–196, 2018.

[55] R. L. Peyton, C. J. Gantzer, S. H. Anderson, B. A. Haeffner, and P. Pfeifer, "Fractal dimension to describe soil macropore structure using X ray computed tomography," *Water Resources Research*, vol. 30, no. 3, pp. 691–700, 1994.

[56] L. Luo, H. Lin, and P. Halleck, "Quantifying soil structure and preferential flow in intact soil using X-ray computed tomography," *Soil Science Society of America Journal*, vol. 72, no. 4, pp. 1058–1069, 2008.

[57] J. Q. Wang, Q. Wang, Y. Y. Kong, Y. Han, and S. K. Cheng, "Analysis of the pore structure characteristics of freeze-thawed saline soil with different salinities based on mercury intrusion porosimetry," *Environmental Earth Sciences*, vol. 79, Article ID 161, 16 pages, 2020.

[58] C. W. W. Ng, D. B. Akinniyi, and C. Zhou, "Influence of structure on the compression and shear behaviour of a saturated lateritic clay," *Acta Geotechnica*, vol. 15, no. 12, pp. 3433–3441, 2020.